Article

-FeO/II–VI Sulfide Nanocrystal Heterojunctions

Kwan-Wook Kwon, and Moonsub Shim

J. Am. Chem. Soc., **2005**, 127 (29), 10269-10275• DOI: 10.1021/ja051713q • Publication Date (Web): 02 July 2005

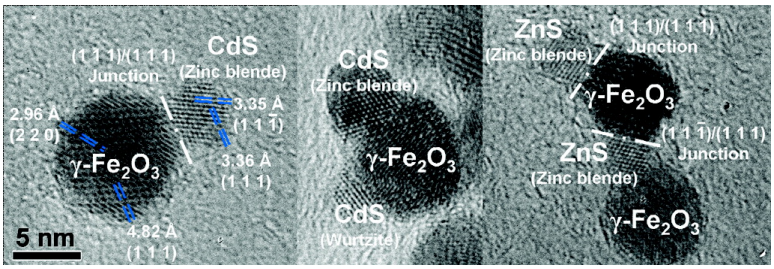

More About This Article

Additional resources and features associated with this article are available within the HTML version:

- Supporting Information
- Links to the 28 articles that cite this article, as of the time of this article download
- Access to high resolution figures
- Links to articles and content related to this article
- Copyright permission to reproduce figures and/or text from this article

View the Full Text HTML

Journal of the American Chemical Society is published by the American Chemical Society. 1155 Sixteenth Street N.W., Washington, DC 20036

J|A|C|S
ARTICLES
Published on Web 07/02/2005

γ-Fe_2O_3/II−VI Sulfide Nanocrystal Heterojunctions

Kwan-Wook Kwon and Moonsub Shim*

Contribution from the Department of Materials Science and Engineering, University of Illinois at Urbana-Champaign, Urbana, Illinois 61801

Received March 17, 2005; E-mail: mshim@uiuc.edu

Abstract: Heterostructure nanocrystals (NCs) of γ-Fe_2O_3 and MS (M = Zn, Cd, Hg) are synthesized. The large lattice mismatch between γ-Fe_2O_3 and MS NCs leads to noncentrosymmetric structures. Crystallographic planes at the heterojunctions are identified by high-resolution transmission electron microscopy. Preferential formation of trimers and higher oligomers for ZnS and dimers or isolated particles for CdS and HgS with γ-Fe_2O_3 NCs are observed and explained by changes in the effective mismatch between the coincidence lattices of the most commonly observed junction planes.

Introduction

Size tunable optical properties, high photoluminescence quantum yields, large surface areas, and versatility afforded by exchangeable surface capping molecules have made semiconductor nanocrystals (NCs) ideal materials for addressing photophysics and chemistry of confined systems as well as for developing novel optical and optoelectronic technologies.[1] Diverse application possibilities including fluorescent labels for biology,[2] light emitting diodes,[3] photovoltaics,[4] and lasers[5] are currently being pursued. A major challenge in realizing many of these technological goals is the controlled assembly of the building block materials. Self-assembly provides a convenient route, but controlling size, size distribution, shape, and surface chemistries of the NCs is critical in achieving desired structures. Initial syntheses[6] have yielded nearly spherical shapes due to the thermodynamic driving force of minimizing surface area, and self-assembly has been limited to the close-packing of spheres.[7] Many recent efforts have led to successful syntheses of NCs with reduced shape symmetry such as rods and tetrapods.[8]

Chemically distinct heterostructures offer further advantages with diversity in self-assembled structures as well as with new opportunities to combine unique properties. However, most efforts in the synthesis of NC heterostructures have been limited to core/shell types where the symmetry of the core is maintained.[9] Heterostructures of NCs with two or more distinct compositions that have noncore/shell geometries with reduced symmetry may facilitate the introduction of an anisotropic distribution of surface functional groups leading to the possibility of chemically programmed assembly of NCs. Separate control of size and shape of each component will lead to a rich phase diagram analogous to block copolymers.[10] Dimers or oligomers of different inorganic materials may also give rise to a combination of unique properties (e.g., magnetic with semiconducting behavior).

Recently, there have been a few reports of formation of bifunctional dimer NCs where two NCs of different inorganic compositions are fused together. Metal−metal (Au−Ag and FePt−Ag),[11] metal-semiconductor (FePt−CdS),[12] and metal−metal oxide (Au−Fe_3O_4 and Ag−Fe_3O_4)[11,13] junctions in NC heterostructures have been shown. Similar heterojunction interfaces are also present in CdTe,[14] Au,[15] or PbSe[16] NCs grown at the tips of CdSe nanorods or tetrapods as well as in semiconductor nanowires[17] and nanowire heterostructures[18] synthesized using metal nanoparticle catalysts. Many of these systems impose interfaces between materials with large lattice

(1) (a) Wang, Y.; Herron, N. *J. Phys. Chem.* **1991**, *95*, 525. (b) Alivisatos, A. P. *Science* **1996**, *271*, 933. (c) Ashoori, R. *Nature* **1996**, *379*, 413. (d) Shim, M.; Guyot-Sionnest, P. *Nature* **2000**, *407*, 981. (e) Klimov, V. I. *J. Phys. Chem. B* **2000**, *104*, 6112. (f) Wang, C.; Shim, M.; Guyot-Sionnest, P. *Science* **2001**, *291*, 2390. (g) Wehrenberg, B. L.; Guyot-Sionnest, P. *J. Am. Chem. Soc.* **2003**, *125*, 7806.
(2) (a) Alivisatos, A. P. *Nat. Biotechnol.* **2004**, *22*, 47. (b) Wang, D. Y.; Rogach, A. L.; Caruso, F. *Nano Lett.* **2002**, *2*, 857.
(3) (a) Colvin, V. L.; Schlamp, M. C.; Alivisatos, A. P. *Nature* **1994**, *370*, 354. (b) Dabbousi, B. O.; Bawendi, M. G.; Onitsuka, O.; Rubner, M. F. *Appl. Phys. Lett.* **1995**, *66*, 1316. (c) Tessler, N.; Medvedev, V.; Kazes, M.; Kan, S. H.; Banin, U. *Science* **2002**, *295*, 1506.
(4) (a) O'Regan, B.; Grätzel, M. *Nature* **1991**, *353*, 737. (b) Nozik, A. J. *Physica E* **2002**, *14*, 115. (c) Schaller, R. D.; Klimov, V. I. *Phys. Rev. Lett.* **2004,** *92*, 186601.
(5) Eisler, H. J.; Sundar, V. C.; Bawendi, M. G.; Walsh, M.; Smith, H. I.; Klimov, V. *Appl. Phys. Lett.* **2002**, *80*, 4614.
(6) Murray, C. B.; Norris, D. J.; Bawendi, M. G. *J. Am. Chem. Soc.* **1993**, *115*, 8706.
(7) Murray, C. M.; Kagan, C. R.; Bawendi, M. G. *Science* **1995**, *270*, 1335.
(8) (a) Manna, L.; Scher, E. C.; Alivisatos, A. P. *J. Am. Chem. Soc.* **2000**, *122*, 12700. (b) Peng, Z. A.; Peng, X. *J. Am. Chem. Soc.* **2002**, *124*, 3343. (c) Gole, A.; Murphy, C. J. *Chem. Mater.* **2004**, *16*, 3633.
(9) (a) Hines, M. A.; Guyot-Sionnest, P.; *J. Phys. Chem.* **1996**, *100*, 468. (b) Dabbousi, B. O.; Rodriguez-Viejo, J.; Mikulec, F. V.; Heine, J. R.; Mattoussi, H.; Ober, R.; Jensen, K. F.; Bawendi, M. G. *J. Phys. Chem. B* **1997**, *101*, 9463. (c) Peng, X.; et al. *J. Am. Chem. Soc.* **1997**, *119*, 7019. (d) Li, J. J.; Wang, Y. A.; Guo, W. Z.; Keay, J. C.; Mishima, T. D.; Johnson, M. B.; Peng, X. G. *J. Am. Chem. Soc.* **2003**, *125*, 12567.
(10) (a) Fredrickson, G. H.; Bates, F. S. *Annu. Rev. Mater. Sci.* **1996**, *26*, 501. (b) Johnson, B. K.; Prud'homme, R. K. *Phys. Rev. Lett.* **2003**, *91*, 118302. (c) Leclere, P.; Calderone, A.; Marsitzky, D.; Francke, V.; Geerts, Y.; Mullen, K.; Bredas, J. L.; Lazzaroni, R. *Adv. Mater.* **2000**, *12*, 1042.
(11) Gu, H.; Yang, Z.; Gao, J.; Chang, C. K.; Xu, B. *J. Am. Chem. Soc.* **2005**, *127*, 34.
(12) Gu, H.; Zheng, R.; Zhang, X.; Xu, B. *J. Am. Chem. Soc.* **2004**, *126*, 5664.
(13) Yu, H.; Chen, M.; Rice, P. M.; Wang, S. X.; White, R. L.; Sun, S. *Nano Lett.* **2005**, *5*, 379.
(14) Milliron, D. J.; Hughes, S. M., Cui, Y.; Manna, L.; Li, J.; Wang, L.-W.; Alivisatos, A. P. *Nature* **2004**, *430*, 190.
(15) Mokari, T.; Rothenberg, E.; Popov, I.; Costi, R.; Banin, U. *Science* **2004**, *304*, 1787.
(16) Kudera, S.; Carbone, L.; Casula, M. F.; Cingolani, R.; Falqui, A.; Snoeck, E.; Parak, W. J.; Manna, L. *Nano Lett.* **2005**, *5*, 445.

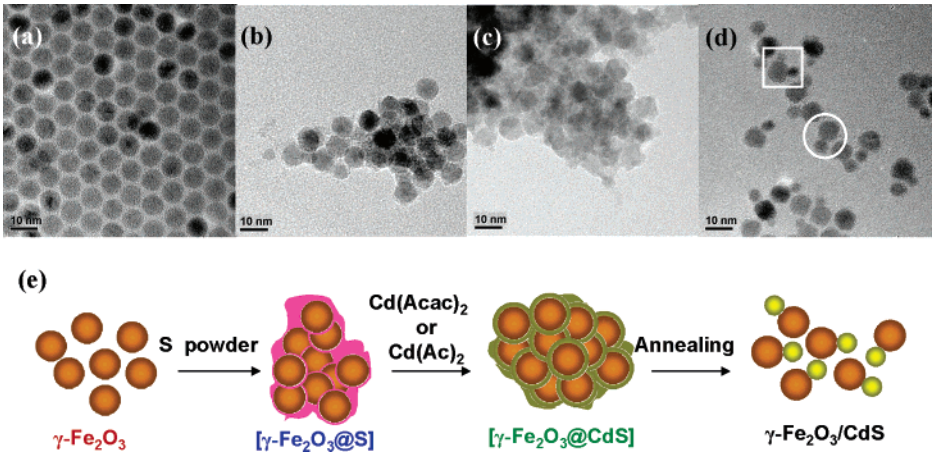

Figure 1. TEM images of the reaction mixture at different stages of the reaction. (a) γ-Fe_2O_3 NCs, (b) γ-Fe_2O_3 NCs after addition of sulfur powder, (c) γ-Fe_2O_3 NCs after addition of sulfur and Cd reagents, and (d) the final heterojunction γ-Fe_2O_3/CdS NCs. A schematic of a possible reaction path to heterojunction NC formation is shown in (e). A typical dimer is circled, and a typical trimer is enclosed in a square in (d).

mismatch, and it is unclear a priori why such junctions should remain intact especially in the presence of excess capping molecules rather than leading to a complete separation to isolated particles. Here, we report on the synthesis of a new subclass of NC heterostructures, metal oxide-semiconductor NCs of γ-Fe_2O_3/MS (M = Zn, Cd, and Hg), and systematically investigate the effects of lattice mismatch on the formation of heterojunctions.

Experimental Section

All syntheses used standard airless techniques. All reagents were used as received. γ-Fe_2O_3 NCs were synthesized by thermal decomposition of iron pentacarbonyl ($Fe(CO)_5$) in the presence of capping molecules similar to the method described in ref 19. After 1.47 mL of oleic acid in 11 mL of octyl ether was vacuum-degassed at 100 °C for at least 30 min, 0.2 mL of $Fe(CO)_5$ was injected under N_2 atmosphere. The reaction mixture was refluxed at $T \sim 290$ °C for 1 h. A small aliquot of the reaction mixture was removed, precipitated with ethanol, and redispersed in chloroform for further analysis prior to the addition of Cd/S reagents.

γ-Fe_2O_3/MS (M = Zn, Cd, Hg) heterojunction NCs were synthesized by direct addition of sulfur and metal reagents to the γ-Fe_2O_3 NC reaction mixture. For γ-Fe_2O_3/CdS NCs, 8 mg of sulfur powder was added to the flask containing crude γ-Fe_2O_3 NC reaction mixture at 100 °C and stirred for 5 min. A solution of 80 mg cadmium acetyl acetonate, 300 mg of 1,2-hexadecanediol, and 400 mg of trioctylphosphine oxide (TOPO) in 1 mL of octyl ether which was vacuum-dried previously at 100 °C was then injected dropwise at 80 °C. After 10 min of stirring at 80 °C, temperature was raised to 230−280 °C. The reaction mixture was allowed to anneal by stirring at the elevated temperature for a few min to several hours. Nearly identical results were obtained when cadmium acetate without 1,2-hexadecanediol was used instead of cadmium acetyl acetonate. γ-Fe_2O_3/ZnS heterojunction NCs were synthesized with the same method as that for γ-Fe_2O_3/CdS by replacing cadmium acetyl acetonate with molar equivalents of zinc acetate without 1,2-hexadecanediol. γ-Fe_2O_3/HgS heterojunction NCs were synthesized by the same method as that for the ZnS system by substituting molar equivalents of mercury acetate and trimethylsilyl sulfide (TMS_2S) as the Hg/S reagents and a lower annealing temperature of 150 °C. The reaction conditions were optimized (in terms of yield of heterojunctions) by varying the final annealing temperature and time for each set of metal and sulfur reagents. Various combinations of reagents for metal (e.g., cadmium acetate, dimethyl cadmium, and cadmium acetyl acetonate for CdS) and sulfur (sulfur powder and TMS_2S) sources were compared. The conditions that led to the highest yield of γ-Fe_2O_3/MS junction formation described above were used for comparison between different heterojunction NCs. The final products were obtained by precipitating the NCs with methanol or ethanol and then redissolving in hexanes or chloroform. For comparison, isolated CdS, ZnS, and HgS NCs were also synthesized by the same respective methods described above in the absence of γ-Fe_2O_3 NCs.

Transmission electron microscopy (TEM) samples were prepared on Cu grids with thin carbon film from a dilute solution of NCs in chloroform. TEM analysis was carried out with JEOL 2010 TEM operating at 200 kV. Rigaku Geigerflex with the D-MAX system was used for the acquisition of powder X-ray diffraction patterns. UV−vis absorption spectra were obtained with Agilent 8453 photodiode array spectrometer.

Results and Discussion

The synthesis of heterostructure NCs that deviate significantly from centrosymmetric core/shell type structures may offer a diverse set of building blocks for self-assembly of interesting architectures. In heterostructure NCs with similar lattice constants,[14] interface formation, and therefore epitaxial growth, is not surprising. However, in large lattice mismatched systems, it is unclear why potentially highly strained interfaces should form when excess capping molecules are present. Furthermore, heterostructure NCs, whether lattice matched or not, may suffer from a wide distribution of geometries that may be difficult to control. For example, a system that forms dimers or trimers may easily form higher oligomers. Figure 1d shows a typical TEM image of NC heterostructures of γ-Fe_2O_3/CdS. While there is a relatively high yield of dimers, isolated γ-Fe_2O_3 and CdS NCs, trimers, tetramers, etc. can also be observed. We refer to γ-Fe_2O_3 particles with one fused MS NC as dimers. We define a trimer as a γ-Fe_2O_3 NC fused with two MS NCs or a MS NC fused with two γ-Fe_2O_3 particles. Oligomers are defined here as any system that has three or more particles fused together. To address why large lattice mismatched interfaces should form stable junctions and to optimize the yield of desired geometry, we examine a series of heterostructure NCs of γ-Fe_2O_3 and II−VI sulfides. ZnS, CdS, and HgS are compared since all three systems can be synthesized under similar conditions and contain

(17) (a) Grebinski, J. W.; Hull, K. L.; Zhang, J.; Kosel, T. H.; Kuno, M. *Chem. Mater.* **2004**, *16*, 5260. (b) Yu, H.; Li, J.; Loomis, R. A.; Gibbons, P. C.; Wang, L.-W.; Buhro, W. E. *J. Am. Chem. Soc.* **2003**, *125*, 16168.
(18) Wu, Y.; Xiang, J.; Yang, C.; Lu, W.; Lieber, C. M. *Nature* **2004**, *430*, 61.
(19) Hyeon, T.; Lee, S. S.; Park, J.; Chung, Y.; Na, H. B. *J. Am. Chem. Soc.* **2001**, *123*, 12798.

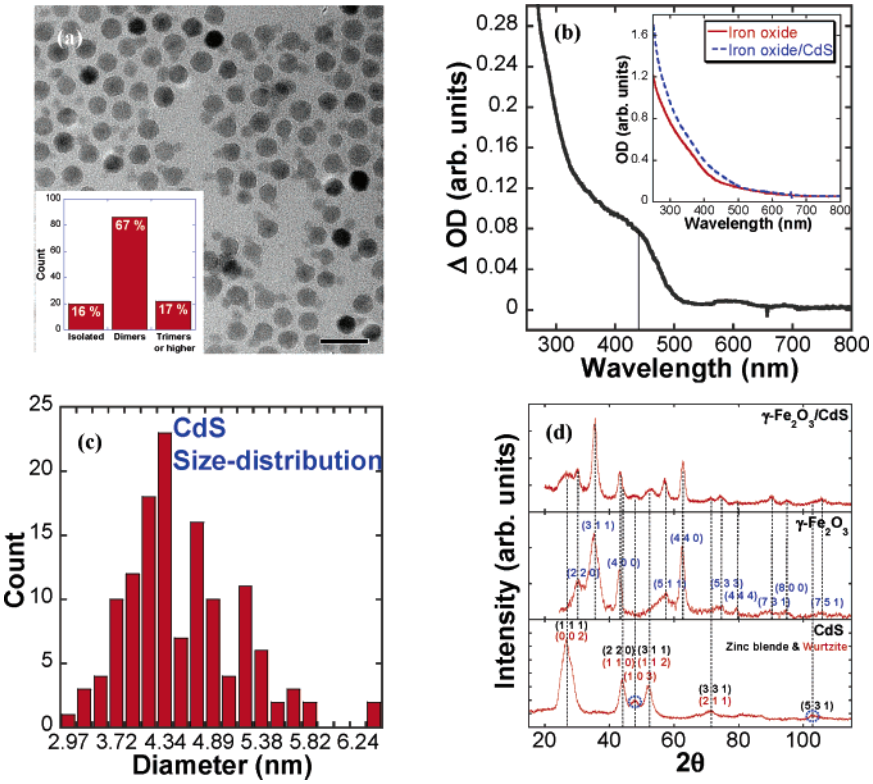

Figure 2. (a) Representative low resolution TEM image of γ-Fe_2O_3/CdS after a crude size selective precipitation. The scale bar is 20 nm. Inset is the distribution of isolated single particles, dimers, and trimers or higher oligomers. (b) Difference spectrum of UV−vis between γ-Fe_2O_3 and γ-Fe_2O_3/CdS solutions. Inset is the UV−vis spectrum of γ-Fe_2O_3 (solid line) and γ-Fe_2O_3/CdS (dashed line), respectively. (c) Size distribution of CdS particles in γ-Fe_2O_3/CdS system. (d) Powder X-ray diffraction patterns of γ-Fe_2O_3/CdS (upper), γ-Fe_2O_3 (middle), and CdS (lower) NCs. In CdS PXRD, circles at $2\theta = 47.8°$ and $2\theta = 102.8°$ indicate the characteristic peaks for wurtzite and zinc blende, respectively.

the same crystal structure, namely the zinc blende structure. By varying the group II elements, the effects of lattice mismatch at the heterojunctions may be systematically addressed. The γ-Fe_2O_3/CdS system which gives the highest yield of dimers is discussed first to demonstrate the characterization methods including interfacial structural analysis.

γ-Fe_2O_3/CdS System. Figure 1a shows a representative TEM image of γ-Fe_2O_3 NCs. In all cases, we start with an identical synthetic route to γ-Fe_2O_3 NCs. The average diameter of the starting γ-Fe_2O_3 NCs is ∼8 nm. A very narrow size distribution is apparent from the spontaneous close packing. Figure 1b shows the TEM image of the reaction mixture after sulfur powder is added. Partial aggregation occurs as indicated by the TEM image as well as slight turbidity observed in the reaction mixture. Similar aggregates are maintained when the Cd reagent is added as shown in Figure 1c. Upon annealing at elevated temperature (280 °C for the case shown Figure 1), the reaction mixture turns back to transparent solution and isolated dimers of CdS heterostructures are formed as shown in Figure 1d. Note that the heterojunction NCs in Figure 1d have fused junctions, whereas even with aggregation, separation between particles on the order of the capping molecule length can be easily observed when a simple mixture of γ-Fe_2O_3 and CdS NCs prepared separately are mixed and drop dried on TEM grids. Figure 1e shows the schematics of the possible reaction path. Although there are also isolated particles of γ-Fe_2O_3 and CdS (∼16%) as well as trimers or higher oligomers (∼17%), dimers are the most abundant forms (∼67%) after only a crude size selection process as indicated by Figure 2a inset. The yield of dimers directly in the reaction mixture (i.e., when all NCs are precipitated with ethanol and redissolve in chloroform) is about 50%. A higher yield of dimers may be achieved with further size-selective precipitation or other purification processes.

The UV−vis spectra of γ-Fe_2O_3 and γ-Fe_2O_3/CdS are shown in Figure 2b inset. Figure 2b is the difference spectrum which should correspond to the contribution only from CdS NCs. Assuming this to be the case, the band edge transition lies near 440 nm (2.82 eV). This optical band gap is consistent with expectations of an ∼430 nm (2.86 eV) band gap for CdS NCs with an average diameter of 4.6 ± 0.6 nm (Figure 2c) obtained from TEM images. Powder X-ray diffraction (PXRD) patterns of γ-Fe_2O_3/CdS (top), γ-Fe_2O_3 (middle), and CdS (bottom) are presented in Figure 2d. CdS NCs without γ-Fe_2O_3 are synthesized with the same conditions as γ-Fe_2O_3/CdS heterostructure NCs as described in the Experimental Section. Both zinc blende (ZB) and wurtzite (W) structures are apparent in the CdS NCs as indicated by the characteristic peaks at $2\theta = 47.8°$ for (1 0 3) of wurtzite[6,20] and $2\theta = 102.8°$ for (5 3 1) of zinc blende.[21] These two peaks and therefore both crystal structures of CdS are also present in the γ-Fe_2O_3/CdS heterostructures.

Figure 3 shows a high-resolution TEM image of γ-Fe_2O_3/CdS heterostructure NC dimer. Fast-Fourier transform (FFT) diffraction patterns of selected areas for CdS and γ-Fe_2O_3 regions along with the simulated FFTs are also shown. This particular dimer has a zinc blende CdS fused with γ-Fe_2O_3. The observation of dual lattice fringes in both components allows us to assign the exact crystallographic planes and their orienta-

(20) Steckel, J. S.; Zimmer, J. P.; Coe-Sullivan, S.; Stott, N. E.; Bulovic, V.; Bawendi, M. G. *Angew. Chem., Int. Ed.* **2004**, *43*, 2154.
(21) Cao, Y. C.; Wang, J. *J. Am. Chem. Soc.* **2004**, *126*, 14336.

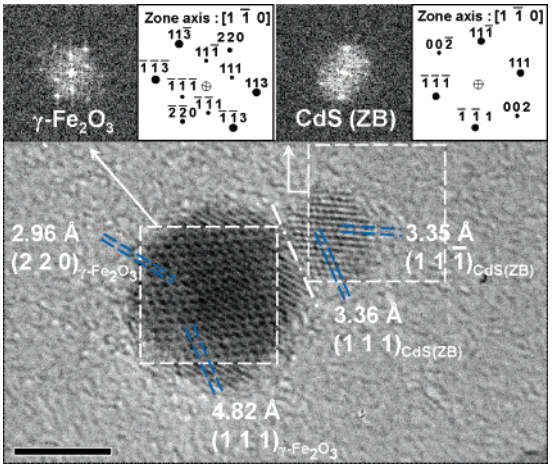

Figure 3. High-resolution TEM image of a γ-Fe_2O_3/CdS dimer. Simultaneous observation of dual lattice fringes for both γ-Fe_2O_3 and CdS parts allow determination of the junction planes and their respective orientations. FFT patterns obtained for γ-Fe_2O_3 and CdS parts separately from the area of square outlines are compared with the simulated FFT patterns obtained with the same zone axes of [1 $\bar{1}$ 0] determined from the crystallographic directions observed from the dual lattice fringes. The scale bar is 5 nm.

tions for CdS and γ-Fe_2O_3 at the junction. From the measured *d* spacing in Figure 3, (1 1 1) and (2 2 0) planes are assigned to the observed lattice fringes for γ-Fe_2O_3. The zone axis (i.e., axis perpendicular to the image) is calculated from the cross product of the two vectors perpendicular to these two planes. The measured FFT pattern of γ-Fe_2O_3 agrees well with the simulated FFT pattern as shown in Figure 3. From this analysis, the junction plane for γ-Fe_2O_3 is assigned to be (1 1 1) with the [1 $\bar{1}$ 0] zone axis. The same analysis on the CdS part leads to the (1 1 1) junction plane with the [1 $\bar{1}$ 0] zone axis. This pair of (1 1 1)$_{\gamma-Fe_2O_3}$/(1 1 1)$_{CdS}$ with the same zone axes [1 $\bar{1}$ 0] is the majority of the interfaces observed (~77%, 20 out of 26 junctions analyzed). Other junction plane pairs observed are (1 1 1)$_{\gamma-Fe_2O_3}$/(1 0 0)$_{CdS}$, (1 1 1)$_{\gamma-Fe_2O_3}$/(1 1 0)$_{CdS}$, (1 0 0)$_{\gamma-Fe_2O_3}$/(1 0 0)$_{CdS}$, and (1 1 0)$_{\gamma-Fe_2O_3}$/(1 0 0)$_{CdS}$ for zinc blende CdS.

Consistent with PXRD results, high-resolution TEM analysis of γ-Fe_2O_3/CdS heterostructures reveal both zinc blende and wurtzite structures of CdS to be present and fused with γ-Fe_2O_3. Interestingly, trimers that have both zinc blende and wurtzite CdS particles grown on a single γ-Fe_2O_3 NC can be observed (Figure 4). From the same junction plane analysis as described for the zinc blend CdS, we find that the predominant junction planes for γ-Fe_2O_3/wurtzite CdS is (1 1 1)$_{\gamma-Fe_2O_3}$/(1 0 $\bar{1}$ 1)$_{CdS}$. This junction is ~65% of 26 junction planes analyzed for the wurtzite case.

Although our results seem to suggest that there may be a preferential combination of crystallographic planes that will form the heterojunctions, more statistics are needed to ascertain such a claim. To fully determine the junction planes and their relative alignment, heterostructure NCs need to be oriented such that dual lattice fringes are simultaneously observable. The total number of such a scenario is rather limited. Furthermore, the junction plane of γ-Fe_2O_3 seems to be dominated by the (1 1 1) plane which is most likely due to this close-packed plane being the most favorable surface termination prior to M/S reagent addition. Therefore, we compare yields of junctions formed on γ-Fe_2O_3 NCs with ZnS, CdS, and HgS (which have systematically increasing lattice parameters) to examine the effects of lattice mismatch. However, the well-aligned crystal-

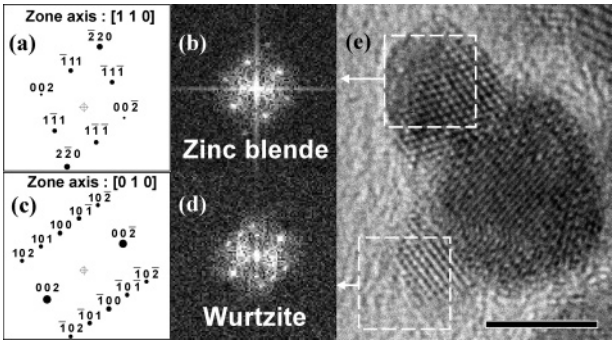

Figure 4. High-resolution TEM image of γ-Fe_2O_3/CdS trimer with two CdS parts on a single γ-Fe_2O_3 NC. FFT patterns are obtained for upper and lower CdS parts from the areas identified by the dotted squares. Interestingly, both zinc blende and wurtzite structures of CdS can grow on a single γ-Fe_2O_3 NC. From the dual lattice fringes in both components, the zone axes are [1 1 0] and [$\bar{1}$ 2 $\bar{1}$ 0] for zinc blende and wurtzite components, respectively. The crystallographic directions and planes for the hexagonal wurtzite CdS are identified with three-coordinate Miller indices in this figure for convenience. FFT patterns simulated with these zone axes compare well with the experimental FFT patterns. The scale bar is 5 nm.

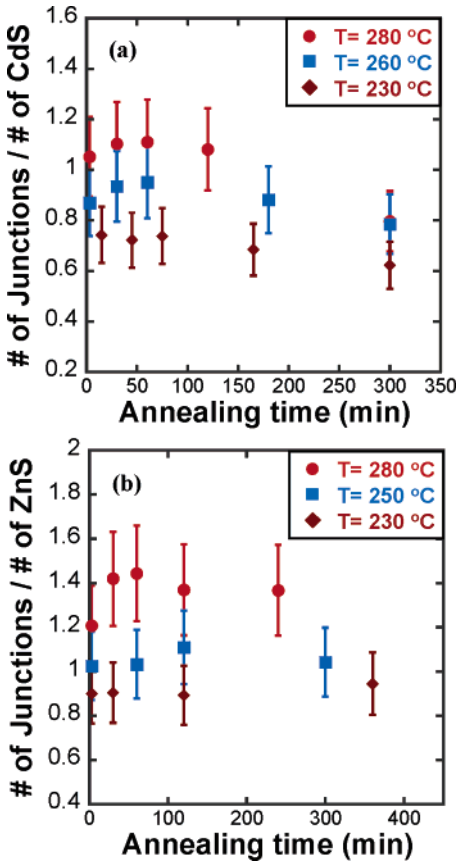

Figure 5. Heterojunction yield normalized to the number of II−VI particles formed at different annealing temperatures and times for optimization of synthesis conditions for (a) CdS and (b) ZnS heterostucture NCs.

lographic directions consistent with low index plane interface terminations suggest epitaxial growth of CdS on γ-Fe_2O_3 NCs.

Effects of Lattice Mismatch on Heterojunction Formation. γ-Fe_2O_3 has a spinel-type structure where Fe^{3+} ions occupy tetrahedral and octahedral sites of a face-centered cubic lattice of O^{2-} anions with cation vacancies distributed in octahedral sites. The lattice parameter for γ-Fe_2O_3 is 8.35 Å, and that of zinc blende CdS is 5.83 Å. In a lattice matched or small mismatch systems, 2D growth via Frank and van der Merwe

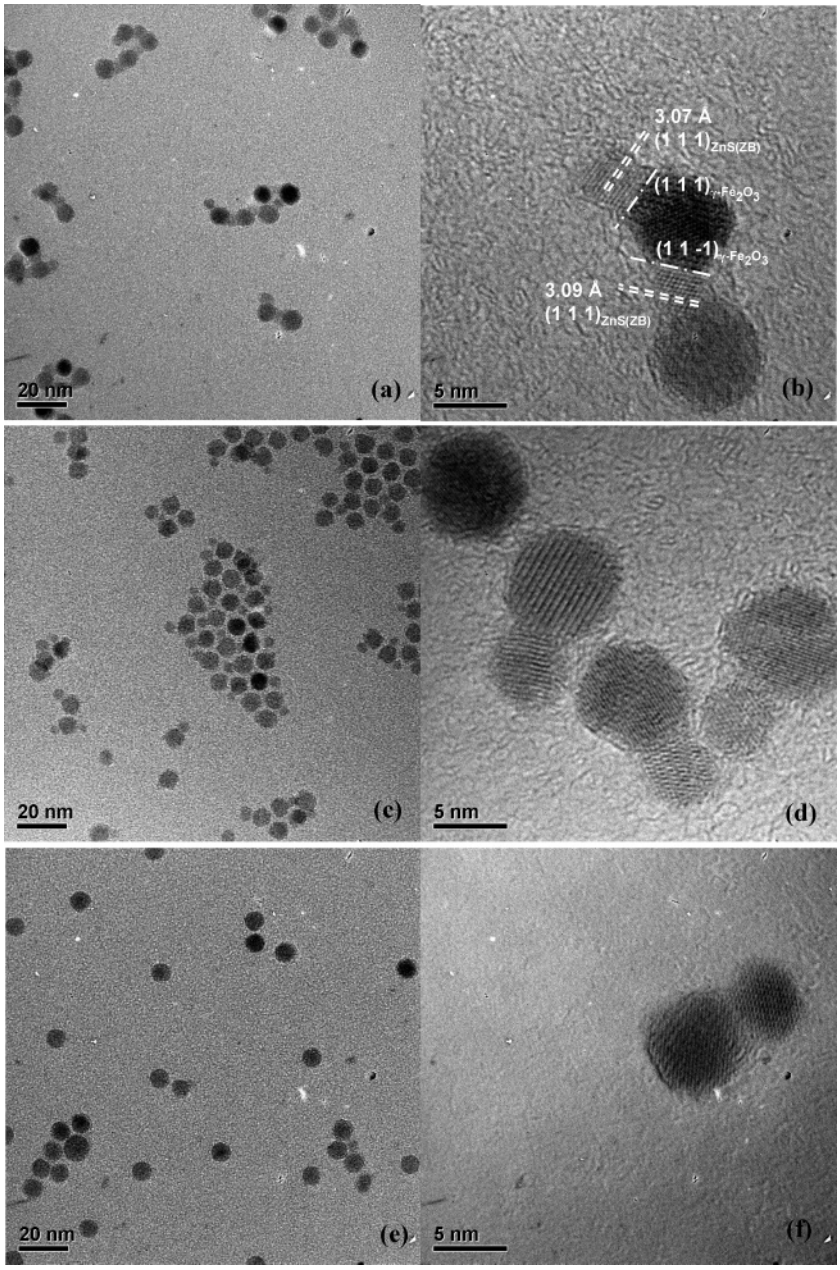

Figure 6. Representative low- and high-resolution TEM images of γ-Fe_2O_3/ZnS (a and b), γ-Fe_2O_3/CdS (c and d), and γ-Fe_2O_3/HgS (e and f) heterojunction NCs without any size-selective precipitation.

mode of growth is expected if the overall surface energy is reduced upon epilayer growth. Such a scenario is likely to lead to core/shell-type structures for the colloidal NCs. In a large lattice mismatched system, mechanism similar to the Volmer−Weber type growth mechanism may explain the formation of noncore/shell heterojunctions. However, in our colloidal systems, since excess coordinating molecules are available to minimize surface energy without inducing significant strain, it seems surprising that fused junctions rather than complete separation of particles occur. It may be even more unexpected that wurtzite CdS which is hexagonal rather than cubic can also form stable heterojunctions.

To investigate how lattice mismatch affects the heterojunction formation in colloidal NCs, we compare the growths of ZnS, CdS, and HgS on γ-Fe_2O_3 NCs. These II−VI semiconductor NCs all have a zinc blende structure (see Supporting Information for PXRD). Similar to CdS, ZnS exhibits both zinc blende and wurtzite structures, but we will limit our discussion to the zinc blende structure. The lattice parameters for these three NCs systematically increase (5.35 Å for ZnS, 5.83 Å for CdS, and 5.85 Å for HgS). Furthermore, similar synthetic conditions can be used which can minimize variations due to differences in the reagent reactivity, capping molecules, etc. Different reagents as described earlier in the Experimental Section have been examined for optimum yields. Temperature and the time of annealing are optimized by counting the number of heterojunctions formed per II−VI particle as shown in Figure 5a and b for CdS and ZnS, respectively. For comparison between systems, we choose the cases where the largest number of heterojunctions per II−VI particle is formed (e.g., heterostructures from annealing conditions of $T = 280$ °C and $t = 1$ h for CdS system).

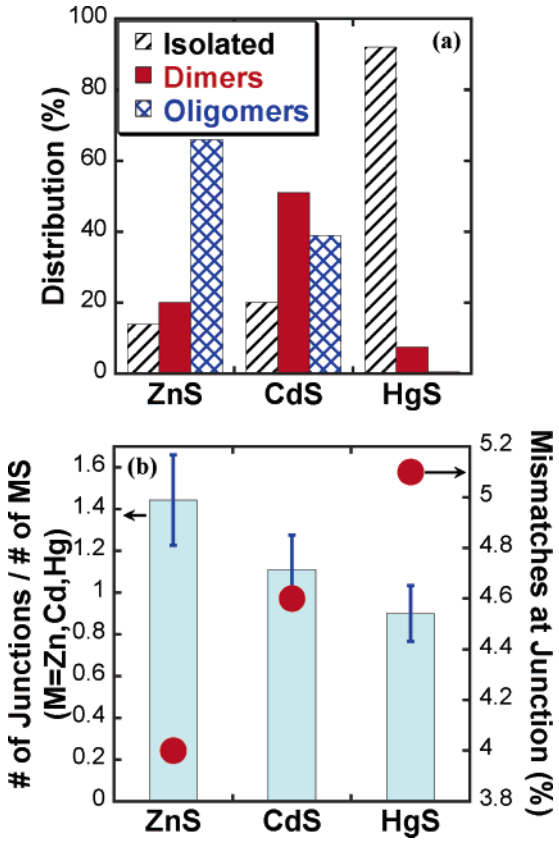

Figure 7. (a) Distribution of isolated single particles, dimers, and higher oligomers for γ-Fe_2O_3/ZnS, γ-Fe_2O_3/CdS, and γ-Fe_2O_3/HgS systems as indicated. (b) Comparison of yield of heterojunction formation normalized to the number of II−VI particles with average effective 2D lattice mismatch for the $(1\ 1\ 1)_{\gamma-Fe_2O_3}/(1\ 1\ 1)_{MS(M=Zn,Cd,Hg)}$ interface as described in the text. Bars are the number of normalized yields, and the filled circles are the effective mismatches.

All comparisons are made on samples that have not undergone any size-selective process.

Figure 6 compares the TEM images of γ-Fe_2O_3 NCs that have formed heterostructures with different II−VI sulfide NCs. To ensure that there are no small semiconductor domains, for example, on top of γ-Fe_2O_3 NCs that we cannot observe with bright field imaging, we have also carried out high-angle annular dark field "Z-contrast" imaging for all three systems (see supporting figures). No detectable amounts of semiconductor domains other than what is visible in the bright field images are observed. Figure 7a shows the distribution of types of NCs formed for the three systems. More than 1000 particles for each system are counted to obtain the distribution shown in Figure 7a. Mostly higher oligomers (66%) with a relatively small number of isolated particles (14%) and dimers (20%) are observed in the ZnS system. In the CdS system, dimers (51%) are the most commonly observed structures followed by higher oligomers (39%) and isolated particles (20%). Although the overall yield is low, HgS NCs are often found to be in the form of dimers or isolated particles. Note that most of the isolated particle count in the HgS system shown in Figure 7a arises from γ-Fe_2O_3 NCs. The low yield of HgS NCs observed here can complicate the comparison of lattice mismatch effect on the heterostructure formation. However, the yield of junction formation for the HgS system is still quite significant at ~8%. To account for the differences in the yield of semiconductor NC formation, we compare the number of heterojunctions normalized to the number of II−VI particles formed.

We assume the Fe−S, not M−O, interface forms at the junction. This assumption is consistent with the observation that when Cd reagent is added first only isolated CdS NCs form. Cd reagent addition after intentional chemical oxidation[19] of γ-Fe_2O_3 also does not lead to junction formation. Only when sulfur is allowed to react with γ-Fe_2O_3 NCs prior to Cd reagent addition, dimers (or higher oligomers) are observed. There may be different surface relaxation mechanisms that minimize strain[22] as well as differences in the surface capping molecule binding strengths and interfacial chemistries that contribute to the overall energies of the heterojunctions. A comprehensive computational approach is therefore necessary and should be used to quantify the interfacial energies. High level computations of interfaces are beyond the scope of this paper, and we only attempt to give a qualitative explanation for heterojunction formation. We limit our discussion to the potential strain effects due to lattice mismatch here. We assume bulk parameters as a simple measure of relative lattice strain that will be imposed upon junction formation. We also consider only the most commonly observed (1 1 1)/(1 1 1) interface with the both crystals having the same zone axis. That is, we will examine how the atoms match up in the experimentally determined interface.

For each junction plane, we define a 2D unit cell as demonstrated in Scheme 1. As shown in the left-most diagram, the 2D unit cell lattice parameters are $a_{\gamma-Fe_2O_3} = 10.23$ Å and $b_{\gamma-Fe_2O_3} = 5.91$ Å for the Fe^{3+} ions on the (1 1 1) plane of γ-Fe_2O_3. The corresponding 2D lattice parameters for S^{2-} anions on the (1 1 1) plane of zinc blende CdS are 7.14 and 4.12 Å. When the two planes are brought together, a new 2D unit cell needs to be defined as shown in the right-most diagram in Scheme 1. Since the new unit cell contains two original 2D unit cells of Fe^{3+} and three original 2D unit cells of S^{2-} along the a direction, we define an effective lattice mismatch as $|(2a_{\gamma-Fe_2O_3} - 3a_{CdS})/2a_{\gamma-Fe_2O_3}| = 4.6$ %. Similarly, the mismatch along b is $|(2b_{\gamma-Fe_2O_3} - 3b_{CdS})/2b_{\gamma-Fe_2O_3}| = 4.6$ %, giving an average 2D lattice mismatch of 4.6%. Using the same method, average 2D lattice mismatches of 4.0% and 5.1% are calculated for ZnS and HgS, respectively. Since there is an increasing mismatch trend, we anticipate decreasing yields of heterojunction formation from ZnS to HgS. The average number of heterojunctions per number of metal sulfide NCs for the three systems shown in Figure 7b indicates that this is indeed the case. The consequence of reduced strain in γ-Fe_2O_3/ZnS is the formation of multiparticle heterostructures, whereas larger lattice mismatches in CdS and HgS systems lead to mainly dimers or isolated particles.

The above geometrical considerations are similar to the basic concepts in the coincidence site lattice model.[23] In large lattice mismatched heteroepitaxial systems and large angle grain boundaries, the coincidence site lattice model has been widely used successfully to explain structures and energies of the interfaces. Incorporation of different interfacial relaxation mech-

(22) (a) Leung, K.; Whaley, K. B.; *J. Chem. Phys.* **1999**, *110*, 11012. (b) Hull, R.; Gray, J.; Wu, C. C.; Floro, J. A. *J. Phys.: Condens. Matter* **2002**, *14*, 12829. (c) Belk, J. G.; Pashley, D. W.; McConville, C. F.; Joyce, B. A.; Jones, T. S. *Surf. Sci.* **1998**, *410*, 82.
(23) (a) Bollmann, W. *Crystal Defects and Crystalline Interfaces*; Springer-Verlag: Berlin, 1970. (b) Brockman, A.; Balluffi, R. W. *Acta Metallurgica* **1981**, *29*, 1703. (c) Trampert, A.; Ploog, K. H. *Cryst. Res. Technol.* **2000**, *35*, 793. (d) Li, B. Q.; Zuo, J.-M. *Surf. Sci.* **2002**, *520*, 7.

Scheme 1. Atomic Arrangement and Definition of 2D Lattice Parameters for Fe^{3+} and S^{2-} on (1 1 1) Planes and the New 2D Unit Cell upon Junction Formation

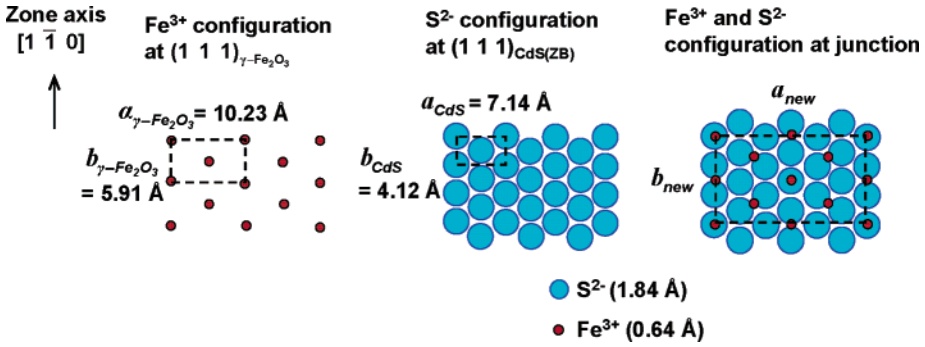

anisms and effects of chemical composition will be required to quantify the heterojunction interfacial energies and therefore to fully explain the reason for heterojunction formation with a significant preference for the (1 1 1)/(1 1 1) interface with the same zone axes in our case. However, our observations are consistent with best matched coincidence lattice systems leading to the highest yield for heterojunction formation. While a comprehensive computation will be necessary to verify, these results give an intuitive, albeit qualitative, explanation of why our systems form noncore/shell-type heterostructures. These results also suggest the possibility of engineering geometries of NC heterostructures by varying the degree of lattice mismatch. We further emphasize that there may be other factors such as differences in the capping ligand affinities, interfacial chemistry, and the electronic structures of NCs that have significant contributions to the overall formation energies of the heterojunction NCs. We have not yet observed qualitative differences by changing the surface capping molecules (i.e., replacing TOPO) in our preliminary studies. Further studies are needed to determine the contributions from factors other than lattice strain and are currently being carried out.

Conclusion

γ-Fe_2O_3/MS (M= ZnS, CdS, HgS) NC heterostructures have been synthesized by a simple one-pot solution process. Both zinc blende and wurtzite structures of CdS as well as ZnS have been observed to grow on γ-Fe_2O_3 NCs. We have identified crystallographic planes at the heterjunctions with the (1 1 1)$_{\gamma-Fe_2O_3}$/(1 1 1)$_{MS}$ interface being the most frequently observed junctions. Systematic increase in the lattice spacing from ZnS to HgS has allowed us to examine how heterojunction structures evolve with increasing lattice mismatch. While other factors such as chemistry at the junction planes and affinity of capping molecules to different MS NCs will contribute to the overall interface energy, large lattice mismatch and the presence of coincidence site lattices indicate the importance of lattice strain on the heterojunction NC formation. ZnS NCs with the smallest average 2D lattice mismatch give rise to mainly multijunction particles, whereas complete particle separation with some dimer formation is observed in the HgS system with the largest mismatch. Dimers are the most abundant species in the γ-Fe_2O_3/CdS system. These results provide insights into heterostructure formation in large lattice mismatched systems and how different geometries (e.g., dimers, trimers, etc.) may be synthesized by varying the lattice parameters of each crystalline component.

Acknowledgment. We thank Dr. Jianguo Wen and Prof. Jian-Min Zuo for helpful discussions and Dr. Changhui Lei and Dr. Heedon Hwang for assistance with High Angle Annular Dark Field (HAADF) "Z-contrast" images. This work was supported by the NSF (Grant No. DMI-0322299). Transmission electron microscopy and X-ray diffraction of the samples were carried out at the Center for Microanalysis of Materials, University of Illinois, which is partially supported by the U.S. Department of Energy under Grant DEFG02-91-ER45439.

Supporting Information Available: Powder X-ray diffraction patterns (γ-Fe_2O_3/ZnS, ZnS, γ-Fe_2O_3/HgS, and HgS NCs) and high-angle annular dark field TEM images with brightness profiles. This material is available free of charge via the Internet at http://pubs.acs.org.

JA051713Q